Earth and Planetary Science Letters 498 (2018) 237–246

Contents lists available at ScienceDirect

Earth and Planetary Science Letters

www.elsevier.com/locate/epsl

Unraveling histories of hydrothermal systems via U–Pb laser ablation dating of skarn garnet

Michelle Gevedon [a,*], Spencer Seman [a,1], Jaime D. Barnes [a], Jade Star Lackey [b], Daniel F. Stockli [a]

[a] Department of Geological Sciences, University of Texas at Austin, Austin, TX 78712, USA
[b] Geology Department, Pomona College, Claremont, CA 91711, USA

ARTICLE INFO

Article history:
Received 22 September 2017
Received in revised form 11 June 2018
Accepted 27 June 2018
Available online 11 July 2018
Editor: M. Bickle

Keywords:
andradite
skarn
geochronology
garnet
hydrothermal system
Sierra Nevada

ABSTRACT

Skarns are one of the few direct genetic links between magma and base metals in ore deposits, yet temporal relationships between skarns and their assumed causative plutons are rarely confirmed with radiometric formation ages. Skarns have been notoriously difficult to date directly due to a limited primary mineral assemblage, generally garnet and pyroxene. Discrepancies in timescales of skarn formation versus pluton emplacement emphasize our tenuous understanding of temporal relationships between plutons and hydrothermal systems including the duration of hydrothermal activity and skarn mineral growth rates. Here we apply a new method for U–Pb dating grossular-andradite (grandite) garnet via LA-ICP-MS and present the first comprehensive study to focus on U–Pb dates of primary skarn garnet. We present U–Pb age constraints on garnets from multiple skarns within the Jurassic and Cretaceous arcs of the North American Cordillera. Two case studies (Darwin and Empire Mountain skarns) illustrate the effectiveness of the U–Pb grandite method by demonstrating that garnet U–Pb ages agree within error of the pluton- and skarn-hosted U–Pb zircon ages. Two additional study localities (Black Rock and Mojave skarns) demonstrate the ability of grandite U–Pb ages to: 1) directly identify a causative igneous event, and 2) record timing of major tectonic events, specifically extensional to trans-tensional shifts in the Jurassic Mojave of California.

1. Introduction

Skarns are the calcic garnet- and pyroxene-rich products of decarbonation reactions driven by infiltration or fluxes of water-rich fluids and commonly occur at the interface of igneous bodies intruding carbonate-rich rocks, and frequently host economically valuable base and precious metals (e.g., Mo, W, Cu, Au, and Ag) in ores minerals. Therefore, skarns serve as one of the most direct genetic links between economically important ores and magmas, and provide a glimpse into the process of fluid and thermal transfer between magma bodies and the surrounding crust. Despite their economic importance, absolute formation ages of skarns are notoriously difficult to determine; as such, few measurements exist on the growth rates of skarn minerals, the duration of skarn formation, or the longevity of hydrothermal activity (e.g., Meinert et al., 2005).

Skarn formation ages are commonly referenced to the crystallization ages of assumed causative intrusive igneous bodies (Nokleberg, 1981; Meinert, 1993; Xie et al., 2011); however, this is problematic in instances where the causative pluton is unknown or ambiguous (e.g. Tornos et al., 2000). Additionally, modern interpretations of magma emplacement emphasizes the potential for pluton emplacement to occur incrementally over several million years (Coleman et al., 2004; Miller et al., 2007), yet thermodynamic models of skarn formation require much less time, on the order of 10^6 to as few as 10^4 years depending on factors such as intrusion size, host rock permeability and conductive vs. convective heat flow (Cathles et al., 1997). This discrepancy between timescales of emplacement and skarn formation suggests that little is known about the temporal relationships of plutons and their active hydrothermal systems, the longevity of hydrothermal activity, the inter-play of multiple coeval hydrothermal centers, rates of skarn mineral growth, and whether subsequent ore formation follows a lapse in hydrothermal activity (Chesley, 1999).

Numerous skarn minerals have been employed as geochronometers (e.g. Re–Os dating of molybdenite veins, and U–Pb dating of accessory allanite and vesuvianite) (Romer, 1992; Stein et al., 2001;

* Corresponding author.
E-mail address: mgevedon@utexas.edu (M. Gevedon).
[1] Now at the Department of Geosciences, Pennsylvania State University, University Park, PA 16802, USA.

https://doi.org/10.1016/j.epsl.2018.06.036
0012-821X/

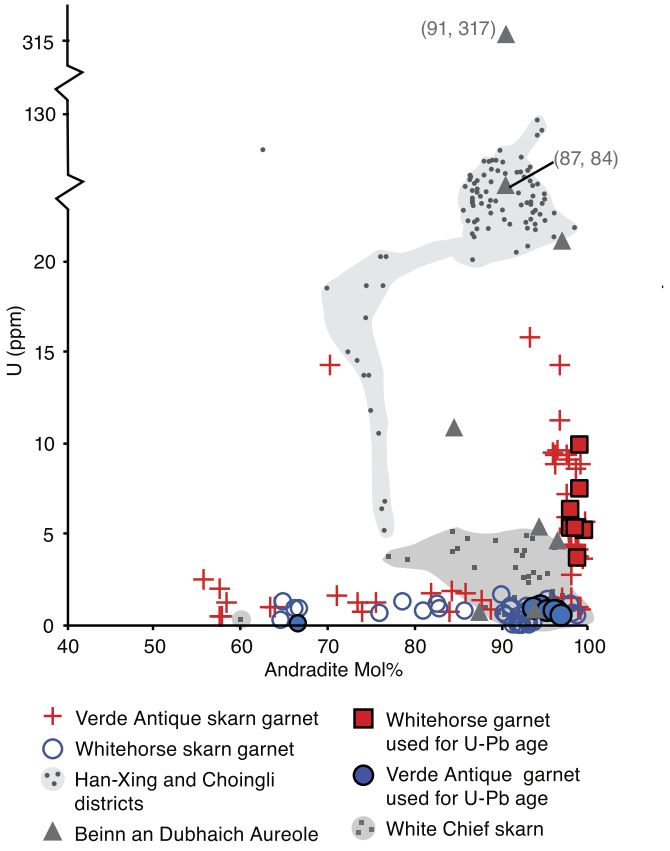

Fig. 1. Plot of measured andradite mol% versus measured U concentration (ppm). Plot depicts a general positive correlation between andradite and U concentration. Individual points represent matched U and andradite compositions; corresponding symbols in solid color represent garnets dated and reported in this study. For reference, the high-U garnets of the Beinn an Dubhaich Aureole19 are shown as triangles (Smith et al., 2004); gray field with square symbols reflects distribution of data from the White Chief skarn, southern Sierra Nevada (Ryan-Davis et al., 2016); light gray fields with circular symbols reflects compositions of the Han-Xing and Choingli districts of the North China craton (Deng et al., 2017).

Mathur et al., 2002; Stein et al., 2003; Deng et al., 2014). Although useful, these methods require the occurrence of accessory mineral phases not universally present in skarns. These methods date the timing of ore formation, which occurs during late-stage metasomatism, or "retrograde" phases of skarn formation instead of at the onset of hydrothermal activity (Meinert et al., 2005). In addition, the inconsistent occurrence of accessory minerals such as metasomatic zircon, xenotime, and monazite keep these minerals from being constant skarn geochronometers (Schaltegger et al., 2005; Rasmussen et al., 2006; Rasmussen and Mortensen, 2013; Liu et al., 2015).

Garnet, however, is common and often voluminous in skarns and is among the earliest, if not the first, of the characteristic paragenetic minerals to crystallize upon skarn formation; these traits mean garnet crystallization most accurately captures the onset of hydrothermal activity. Past attempts to apply the U–Pb geochronometer via TIMS to garnet have been plagued by low concentrations of U (typically <1 ppm) (DeWolf et al., 1996). However, andradite-rich garnets, and andradite-rich zones within grossular garnets, are common in most skarns (Meinert et al., 2005) and have the ability to accommodate U via suspected coupled substitutions involving Fe^{3+} (DeWolf et al., 1996; Smith et al., 2004; Guo et al., 2016), with a common positive correlation between increasing mol% andradite and U concentration (Fig. 1). To date, attempts to date U–Pb skarn garnets are limited to one conference abstract (Meinert et al., 2001) and recent work by Seman et al. (2017) and Deng et al. (2017). However, all of these papers are focused on method development and demonstrating the viability of the method by illustrating garnet U–Pb ages are coeval with pluton age. Here we not only show the viability of the method, but highlight its utility by addressing geologic questions.

The closure temperature of the U–Pb system for a 0.5 cm diameter garnet is estimated to exceed 800 °C though no specific estimates for grossular-andradite garnet exists (Mezger et al., 1989; Burton et al., 1995; DeWolf et al., 1996). However, skarn formation temperatures generally range from 350 to 650 °C (Bowman, 1998), well below the U–Pb closure temperature of garnet. Low formation temperatures of skarn garnet, coupled with the high closure temperature for garnet U–Pb indicates that diffusion is unlikely to affect U–Pb dating of andradite. Despite relatively low [U], andraditic garnet is well suited for laser ablation ICP-MS analysis as it is large, commonly exceeding 500 µm in diameter, and can accommodate large (>60 µm) laser spots.

Here we present two case studies from the Darwin and Empire Mountain skarns demonstrating the effectiveness of a new application of U–Pb LA-ICP-MS geochronometry for dating andradite-rich garnets from natural skarn systems, as well as two additional case studies from the Black Rock Mine and two Mojave Desert skarns demonstrating two different applications of the method: (1) identification of an unknown causative pluton, and (2) generation of temporal constraints on regional hydrothermal alteration and oscillations in the paleo-shoreline of the Jurassic Mojave.

2. Geologic setting of the Mesozoic Cordilleran skarns

This study samples skarns from the Mesozoic North American continental arc, including the Mojave Desert, Inyo and Benton Ranges, and Sierra Nevada, California, which provide a spatial and temporal cross-section of skarn-forming environments through the composite arc (Table 1; Fig. 2). Samples from the Mojave Desert, and Benton and Inyo Ranges sample older (Triassic and Jurassic) inboard portions of the arc where isolated plutons and stocks commonly intruded thick passive margin sedimentary sequences rich in carbonate wallrock (Nelson, 1962; McKee and Conrad, 1996; Saleeby and Dunne, 2015). The Darwin Stock exemplifies such intrusions in that the age of its associated pluton (ca. 175 Ma, Chen and Moore, 1982) lies at a relatively subdued period of magmatism in the Jurassic, and is located over 50 km from another exposed pluton of this age. In addition, significant interest in its Pb, Zn, and Ag mineralization has led to detailed study of the connections between skarn petrogenetic sequences and ores (e.g., Newberry et al., 1991 and references therein). At the Darwin skarn, tungsten-bearing garnet skarn is shown to be early-stage and well-exposed in direct and intermingled contact with the top of the quartz monzonite in the eroded pluton core. Thus this pluton provides an excellent setting to test for linkage between of U–Pb age of skarn garnet and plutonic zircon. In contrast, many Cordilleran arc plutons and associated skarns may be subject to overprinting by extensional deformation and in some cases, younger, regional plutons may lead to considerable skarn formation age uncertainty.

Such is the case for the Cordilleran arc segments of the Mojave where plutons of Triassic, Jurassic, and Cretaceous age are intruded into arc crust that was continually deformed (trans-tension and extension) during the Mesozoic (Walker et al., 1990, 2002). As a result, clear pluton-skarn associations are elusive and further obscured by recent Basin and Range extension. Further complication arises because Mojave arc segments expose shallow crustal levels where hypabyssal intrusions and silicic volcanic deposits range from ca. 180 to 148 Ma (Walker et al., 1990, 2002) and capture an upper-crustal volcanic–plutonic transition. These shallow intrusion levels allowed volumetrically large quantities of surface (meteoric) waters to infiltrate to skarn formation depths within a

Table 1
Locations and sample descriptions.

Sample number	Sample description	Latitude	Longitude
Darwin skarn			
13DW2F *garnet*	Garnet rims from garnetite, averaged	36.277167	117.597014
13DW2F *zircon*	Zircon hosted in skarn garnetite		
Black Rock skarn			
14BR2A_a *garnet*	Garnet from garnetite, *averaged*	37.682125	118.514939
15BR_1 *zircon*	Zircon from peraluminous granite	37.640683	118.516367
15BR_2 *zircon*	Zircon from feldspar-megacrystic granodiorite	37.637997	118.516164
15BR_3 *zircon*	Zircon from quartzmonzonite of Deer Springs	37.648933	118.615775
16BR2 *zircon*	Zircon from biotite granodiorite	37.682758	118.534106
Empire Mountain skarn			
10MD32 *garnet*	Single garnet (rim only) in texturally late quartz vein	36.466403	118.584608
Verde Antique skarn			
14SW2C_cd *garnet*	Single garnet from garnetite	34.669247	117.094931
14SW2C_ce *garnet*	Single garnet from garnetite		
Whitehorse skarn			
15SW3W_a *garnet*	Thick rim of large garnet, garnetite	34.542622	116.962464

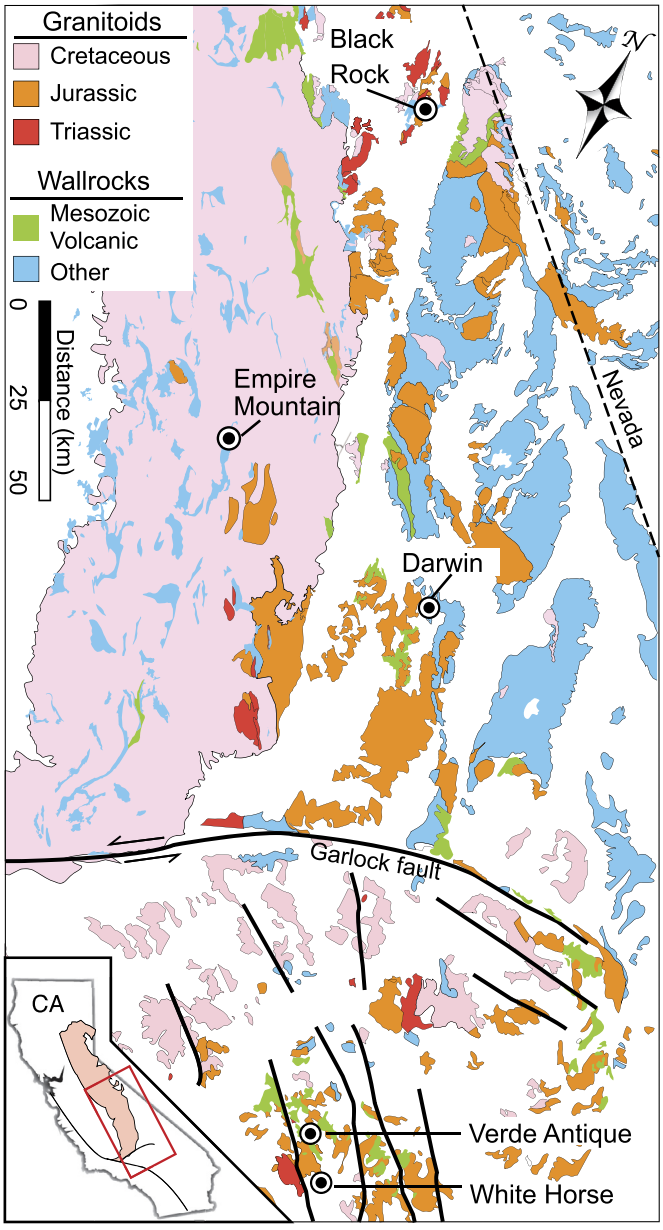

Fig. 2. Map depicting locations of skarns sampled in this study. See Table 1 for GPS coordinates and brief sample descriptions.

large regional hydrothermal system, and resulted in hydrothermal alteration of many plutons and volcanic rocks (Solomon and Taylor, 1991). This alteration affects all regional Jurassic Mojave plutons. Therefore, dating of the skarns in the region (Whitehorse and Verde Antique in this study) provides a robust means to precisely constrain the timing of active meteoric water incursion, which reflects the relationship between changing tectonic regime, plutonic–volcanic expression in the arc, and styles of ore mineralization.

Skarns in the Sierra Nevada arc are the antithesis of the Mojave arc skarns as voluminous Cretaceous plutonic rock far exceeds the proportion of the metamorphic wallrock. Sierra Nevadan skarns are found in scattered wallrock screens often bound by multiple, well-exposed plutons. A multitude of local plutons, however, obfuscates skarn–pluton genetic and age relations, thus making direct dating of skarn minerals particularly powerful for linking hydrothermal activity to specific intrusive events. The case study of the Empire Mountain skarn in the Mineral King pendant of the south-central Cretaceous Sierra Nevada, tests whether garnet skarn formation ages can directly implicate a single intrusion as the source of metasomatizing fluids despite the presence of several different local Cretaceous plutons.

3. Methods

Garnet from all samples, with the exception of Empire Mountain, was removed from whole rock samples either via mechanical means or whole rock dissolution in HCl. Garnet for analyses are sub- to euhedral such that the center of the garnet is easily identifiable, and are ~25 mm or greater in diameter, such that several laser spots may fit within one crystal. Individual garnets chosen for analysis were mounted in 1-inch epoxy rounds, polished to the garnet center, then subsequently polished using 1 µm diamond paste. For the Empire Mount sample, a euhedral garnet was analyzed *in situ* within a ~40 µm thick section.

The ability of grossular-andradite garnet to accommodate measurable concentrations of U is hypothesized to rely on coupled substitutions involving Fe^{3+} (DeWolf et al., 1996; Smith et al., 2004; Guo et al., 2016). Skarn garnets are frequently compositionally-zoned and may alternate between near end-member grossular ($Ca_3Al_2(SiO_4)_3$) and end-member andradite ($Ca_3Fe_2^{3+}(SiO_4)_3$) within a single crystal. The highest precision andradite U–Pb ages reported in this study via laser ablation were attained by characterization of compositional zonation prior to laser ablation in order to identify zones of high Fe^{3+}. High andradite zones were identified either quantitatively through electron probe micro-analyzer (EPMA) determination of X_{And} and X_{Gros}, or qualitatively through SEM energy dispersive X-Ray spectroscopy (EDS) mapping of ap-

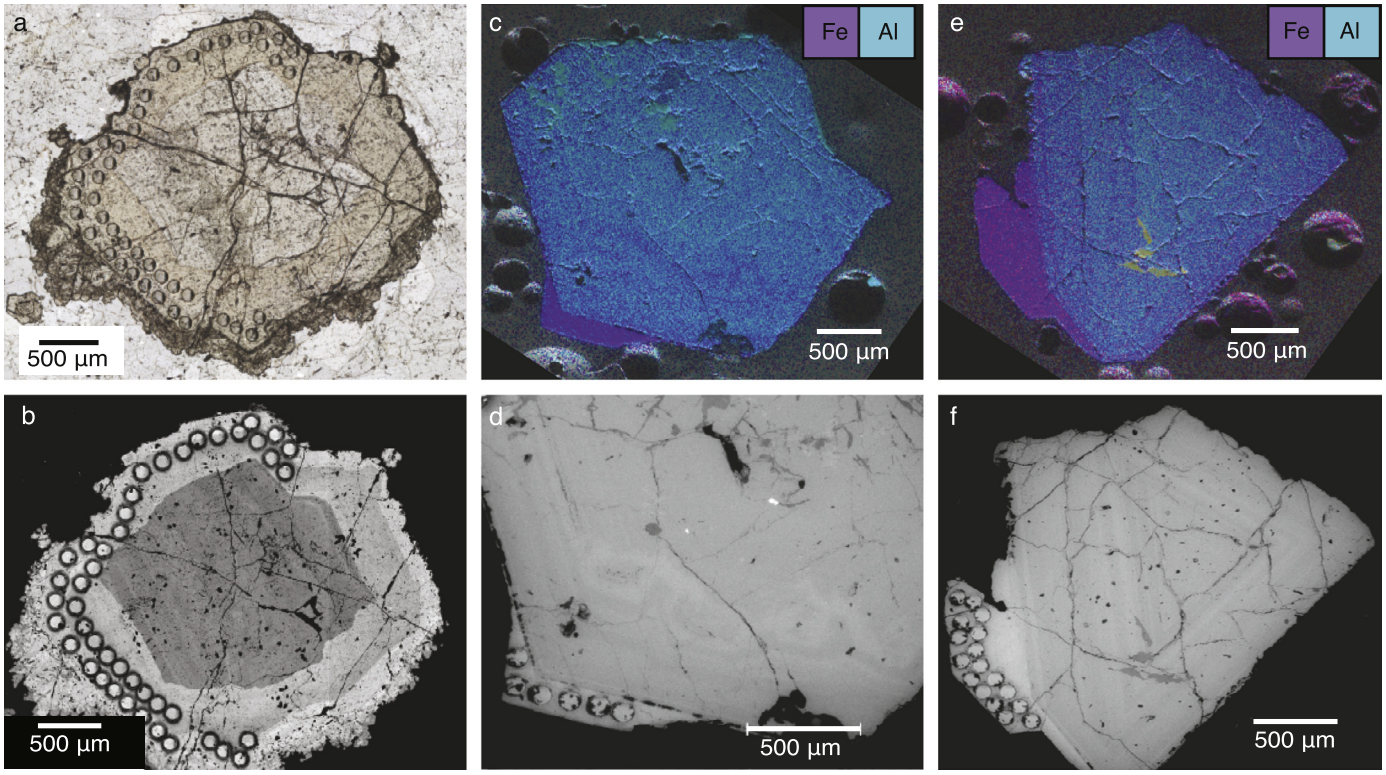

Fig. 3. Visual representation of laser ablation spots corresponding to high-andradite garnet zones. (a) Photomicrograph of visually zoned garnet surrounded by texturally late quartz vein cross-cutting skarn garnetite of the Empire Mountain skarn (10MD32). Circular pits show the placement of laser ablation analyses. (b) Back-scatter electron (BSE) image of same dated Empire Mountain skarn garnet. Brighter hues in BSE correspond to heavier atomic masses; bright inner and outer rims shown are produced by higher concentrations of Fe in the rims than in the core. Laser ablation pits are positioned within these high-Fe rims. (c), (e) Energy dispersive X-ray spectroscopy (EDS) images of Darwin skarn garnets obtained prior to laser ablation and used to identify and target Fe-rich rims. Purple and blue colors indicate emission of X-rays corresponding to Fe (proxy for andradite) and Al (proxy for grossular) respectively. (d), (f) BSE images of same Darwin skarn garnets as shown in figures (c) and (e), respectively. Laser ablation pits correspond with Fe-rich zones as identified by the EDS images.

parent Al:Fe ratios. Both EDS maps and back-scatter electron (BSE) images were made using a Phillips/FEI XL30 environmental scanning electron microscope (ESEM) in low-vacuum mode such that a carbon coat was not required prior to U–Pb analyses; carbon coating was avoided due to the potential of Pb contamination from the carbon source. The measured X_{And} component of all garnets in this study were measured using the JEOL JXA-8200 electron probe micro-analyzer with an accelerating voltage of 25.0 kV and focused beam current of 20 nA at the University of Texas at Austin after U–Pb analyses were complete. Natural and synthetic silicate and oxide standards were used.

All garnet U–Pb age data were collected on a ThermoFisher Element II, single collector, magnetic sector ICP-MS with a Teledyne Analyte G2 193 nm ArF excimer laser and a two-volume Helex cell at the University of Texas at Austin (UTChron Laboratory), following the methods described in Seman et al. (2017). Willsboro Andradite was employed as a primary U–Pb age standard (Fig. DR1); Mali Grandite served as a secondary, quality control standard. A laser spot with a diameter of 110 µm was used to target zones of high-andradite garnet (Fig. 3). Primary standard (Willsboro Andradite) analyses were interspersed between every 5 unknown analyses. Secondary standards were dispersed evenly throughout the analytical session. As the grossular-andradite solid solution incorporates non-radiogenic Pb (Pbc), garnet U–Pb ages are determined using linear regressions in Tera–Wasserburg Concordia (Tera and Wasserburg, 1972). Garnet U–Pb dates are lower intercepts determined by linear regression of discordant arrays. Reported garnet age determinations are based on multiple concordant analyses from one or more individual garnets depending on the size of the garnet (Table 2) as calculated using Isoplot version 3.0. The mean squared weighted deviation (MSWD) of the linear regression through the discordant array is used to assess analyzed garnets which may contain multiple isotopic compositions of Pbc.

Zircon U–Pb ages were determined following the methods described in Levina et al. (2014) and Hart et al. (2016) and using a 30 µm spot. Reported zircon U–Pb analyses have less than 10% discordance between $^{206}Pb/^{238}U$ and $^{207}Pb/^{235}U$ ages; zircon U–Pb ages reported are the one sigma coherent age populations as calculated by Isoplot 3.0.

Careful screening of all garnet samples was done to avoid analysis of inclusions. BSE images and X-ray maps were utilized to avoid surficial exposures of mineral inclusions, and to analyze discrete growth annuli. Although inclusions may be concealed below the exposed mineral surface, positioning the analytical spots within growth zones suggests that any inclusions incorporated into the analysis will be either the same age as the surrounding host garnet, or older than the age of the garnet and be identifiable. Where inclusions were a concern, trace element ratios of the analyzed andradite-rich zones also were used to monitor for the possibility of inclusions within the analyzed garnet zone (see section 5.1.1 as an example).

Trace element data were collected via laser ablation at UTChron Laboratory at the University of Texas using the same instrumentation as used to measure U–Pb ratios. NIST-612 glass served as a primary concentration standard. Trace element analyses used 40 µm laser spots, 10 Hz repetition rate, 30 s of ablation, and 1.67 $J\,cm^2$ fluence; analytical spots were positioned adjacent to the locations of the U–Pb analytical spots and within the same apparent growth annuli in order to characterize the composition of the annulus.

Table 2
Laser ablation U–Pb ages of garnet and zircon.

Sample number	Andradite (mol%)	Garnet [U] (ppm)	U–Pb age (Ma)	Precision[a] (%)	MSWD	Number of garnet	"n"	Corresponding pluton age
Darwin skarn								
13DW2F *garnet*	92 to 98 (rims)	16.9 to 41.2	175 ± 1	2.1	1.9	11	31	175 Ma (Chen and Moore, 1982)
13DW2F *zircon*	–	–	178 ± 3	–	–	–	12	175 Ma (Chen and Moore, 1982)
Black Rock skarn								
14BR2A_a *garnet*	20 to 51 (cores)	1.88 to 17.2	172 ± 3	3.3	5.0	2	87	Causative pluton unknown
15BR_1 *zircon*	–	–	206 ± 2	–	–	–	28	–
15BR_2 *zircon*	–	–	175 ± 1	–	–	–	42	–
15BR_3 *zircon*	–	–	221 ± 2	–	–	–	35	–
16BR2 *zircon*	–	–	211 + 8, −3	–	–	–	17	–
Empire Mountain skarn								
10MD32 *garnet*	46[b] and 62[c]	undetermined	103 ± 4	5.5	3.7	1	41	106 ± 1 (Sisson and Moore, 2013)
Verde Antique skarn								
14SW2C_cd *garnet*	98.1 to 99.7	3.6 to 5.4	161 ± 2	2.8	1.6	1	19	Assumed. Regional ages of 151
14SW2C_ce *garnet*	98.0 to 99.7	5.4	162 ± 2	2.8	1.3	1	17	to 167 Ma (Karish et al., 1993)
Whitehorse skarn								
15SW3W_a *garnet*	93.7 to 96.9	0.5 to 1.0	149 ± 5	4.3	1.5	1	50	Assumed. Regional ages of 151 to 167 Ma (Karish et al., 1993)

[a] Garnet age percent precision including the percent precision of the Willsboro andradite garnet standard TIMS analysis (1022 ± 16 Ma).
[b] Garnet core.
[c] Garnet rim.

4. Results: U–Pb garnet and zircon ages

Skarn garnet successfully U–Pb dated in this study by LA-ICP-MS analysis are characterized by relatively high Fe^{3+} concentrations, but in fact span a range of grossular-andradite composition. One garnet domain that was successfully dated was iron poor (X_{And} as low as 20, garnets analyzed generally range from 40 to >99 mol% andradite (Table 2; Fig. 1). U–Pb ages were determined in garnet growth zones with average $X_{And} > 35$ (Figs. 1 and 2). Calculated lower-intercept ages were derived from multiple ($n \geq 17$) 110 µm laser spot analyses on one or more garnet crystals (Table 2). Garnet domains characterized by lower Pbc typically yielded more precise and reproducible age determinations. Ages from both andradite garnet and metasomatic zircon are presented in Table 2; all uncorrected isotopic data may be found in Tables DR1 and DR2.

5. Discussion

5.1. Case studies

5.1.1. Case study one: Darwin skarn, Argus range

The 175 ± 1 Ma (Chen and Moore, 1982) Darwin stock in eastern California's Argus range has a small size, solitary location, and emplacement age during a lull in arc magmatism. Thus, it would appear to be a simple, short-lived plutonic system, but the preponderance of previous work points to two stages of ore formation, with earlier W ores forming at the pluton contact, and Ag–Zn–Pb skarns forming on faults that cut the intrusion (Newberry et al., 1991). The Darwin Stock presents clear contact relations of the early-stage W-skarns and the pluton. In particular, in the center of the pluton, zircon occurs in the garnet skarn found within 1 m of the top of the pluton and was successfully separated and dated, thus providing a second measure of on the age of the skarn. Collectively, the detailed prior work and two U–Pb phases to target associated with a relatively small pluton makes the Darwin skarn an excellent locale to apply this garnet U–Pb method.

Direct comparison of skarn grandite U–Pb ages with those of garnetite-hosted zircon provide the opportunity to assess the validity and precision of the analytical method. The U–Pb grandite age (175 ± 1 Ma; MSWD = 1.9; Table 2; Fig. 4a) obtained from andradite-rich garnet crystal rims, is in agreement with the ~175 Ma zircon age (Chen and Moore, 1982) of the genetically linked Darwin stock. Moreover, the zircon from the skarn yield a U–Pb age of 178 ± 3 Ma (Table 2; Fig. 4b, Fig. DR2a). This agreement between the previously published Darwin stock age, the newly determined age of the zircon in the tungsten-bearing garnetite, and the age of the Darwin skarn garnet demonstrates the viability of grandite U–Pb as a tool for directly dating skarns.

The presence of zircon within the Darwin garnetite presents the possibility that laser ablation intersected zircon inclusions within the skarn garnet despite careful characterization of the sample surface via SEM. However, trace element ratios of the analyzed andradite-rich zones can be used to screen for inclusions. Trace element concentrations were measured within the andradite-rich garnet rims in order to assess the possible presence or absence of zircon. Trace element concentrations of Zr in ten out of 18 analyses of the Darwin garnet rims are below detection limits (<1 ppm; Fig. 4c). Analytical spots where [Zr] is below the detection limit correspond with higher [U] than analytical spots with measurable [Zr]. If U was hosted by zircon inclusions within the host andradite, the opposite relationship between [Zr] and [U] would be observed. Instead, the trace elements of the Darwin skarn garnet reveal compositional heterogeneity within the garnet rims, perhaps due to the influence of the Darwin Stock magma. Furthermore, both allanite and monazite have structurally controlled Th/U ratios >> 3. Measured Th/U ratios of Darwin skarn andradite rims fall within a range of 0.001 to 0.2 based on the same 18 laser ablation analyses, suggesting that neither monazite or allanite inclusions host the measured U.

The Darwin skarn zircon Th/U ratios (0.4 to 1.2; $n = 12$) suggest they are dominantly magmatic in their character (Hoskin and Schaltegger, 2003). These new age data from both magmatic zircon with texturally late rims of skarn garnetite (Fig. 4a and 4b) permit but do not require close succession of pluton emplacement and the onset of skarn forming hydrothermal activity.

5.1.2. Case study two: Empire Mountain

The skarn at Empire Mountain is readily interpretable as the result of interaction between the shallow, sub-volcanic Empire Mountain pluton and the Mineral King pendant (Fig. 2) despite close proximity to the White Chief skarn and White Chief pluton. The Empire Mountain pluton is well characterized in terms of age, geologic history, and composition (Busby-Spera, 1983; D'Errico et al., 2012; Sisson and Moore, 2013), thereby providing excellent context for determining the accuracy of a skarn grandite age. The grandite U–Pb age of 103 ± 4 Ma (MSWD = 3.7; Table 2; Fig. 5) is

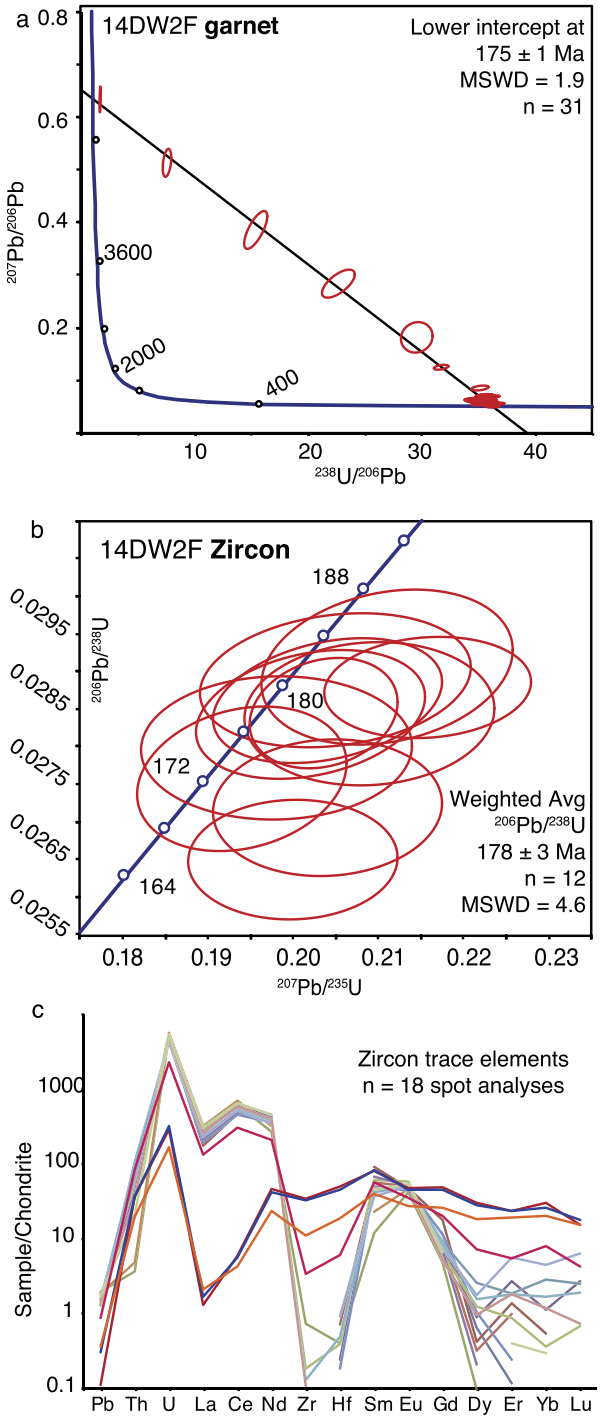

Fig. 4. U–Pb and trace element data pertaining to the Darwin skarn case study. (a) Tera-Wasserberg Concordia (TWC) of garnet U–Pb ages of high-andradite rims of Darwin skarn garnet. All data-point error analyses are 2σ. (b) Wetherill Concordia diagram depicting U–Pb age determination of zircon separated from the Darwin Skarn garnetite. All data-point error analyses are 2σ. (c) Diagram of trace element concentrations of high-andradite rims used to obtain U–Pb age. [Zr] is below detection limit for 10 out of 18 total analyses, these analyses are depicted as open breaks at Zr on the X-axis. When Zr is above detection limits it corresponds with a LREE enrichment inconsistent with addition of LREEs from incorporation of zircon.

within error of the previously reported age of the Empire Mountain pluton, 106 ± 1 Ma (Sisson and Moore, 2013).

Laser ablation on the Empire Mountain skarn sample was conducted as *in situ* analyses on one euhedral, texturally late-stage garnet surrounded by coarse-grained vein quartz (Fig. 5). The ability to conduct *in situ* analyses allows for interpretation of age-data

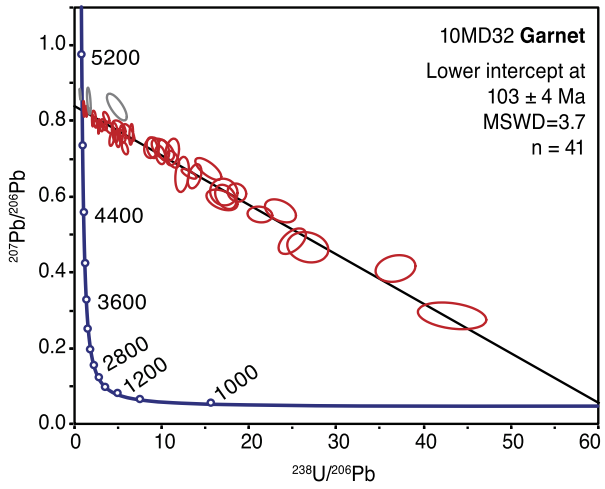

Fig. 5. Tera-Wasserberg Concordia diagram for in situ analysis of Empire Mountain skarn garnet in texturally late quartz vein. Analytical outliers are show in gray and excluded from age calculation. All data-point error analyses are 2σ. (For interpretation of the colors in the figure(s), the reader is referred to the web version of this article.)

in the context of important textural information lost during analysis of a separated mineral. Compositional zonation is observable in plane polarized light, and BSE images and electron probe data confirm the presence of grossular-rich core and andradite-rich rim (Fig. 3b). Internal zonation structure visible within the garnet core suggest at least a 3-step history of this particular garnet: initial growth, resorption or dissolution, followed by additional growth stages (Figs. 3a and 3b). Laser ablation was purposefully restricted to the andradite-rich rim, thus dating the later stages of garnet growth. The inclusion of this garnet within a texturally-late quartz vein cross-cutting the Empire Mountain skarn garnetite further emphasizes that the analyzed garnet is not the product of coeval growth of the main garnetite body, but rather occurred once skarn formation was well established. We interpret the identical ages of this garnet (103 ± 4 Ma) and the Empire Mountain quartz diorite (106 ± 1 Ma) to signify that skarn formation at Empire Mountain, though volumetrically significant and with multiple stages of development and possible protracted time span of skarn formation, occurred concomitant with the emplacement of the Empire Mountain quartz diorite.

5.2. Application of the U–Pb garnet method

5.2.1. Application one: identifying the causative pluton of the Black Rock Mine skarn using grandite U–Pb geochronology

In regions of skarn formation, compound emplacement of multiple local plutons may obscure the identity and age of a skarn's causative pluton (e.g., Tornos et al., 2000). The genetic relationship between the Black Rock Mine skarn (Benton Range, CA) and its causative pluton is not obvious because apparent faulting between the main skarn body and the physically closest pluton (Elliot, 1971; Newberry, 1983) complicate determination of the causative pluton based on field relations. A minimum of four plutonic bodies of various ages present in the immediate region of the Black Rock Mine skarn may have contributed to the fluid and heat budget necessary for skarn formation. Samples were collected from each of these four plutons, which yield weighted-mean zircon U–Pb ages of 221 ± 2 Ma, 211 + 8 and −3 Ma, 206 ± 2 Ma, and 175 ± 1 Ma (Table 2, Figs. 6a to 6d, Figs. DR2b to DR2e). These ages are in good agreement with the age ranges and distribution of Triassic and Jurassic plutons distributed throughout the region (Barth et al., 2011).

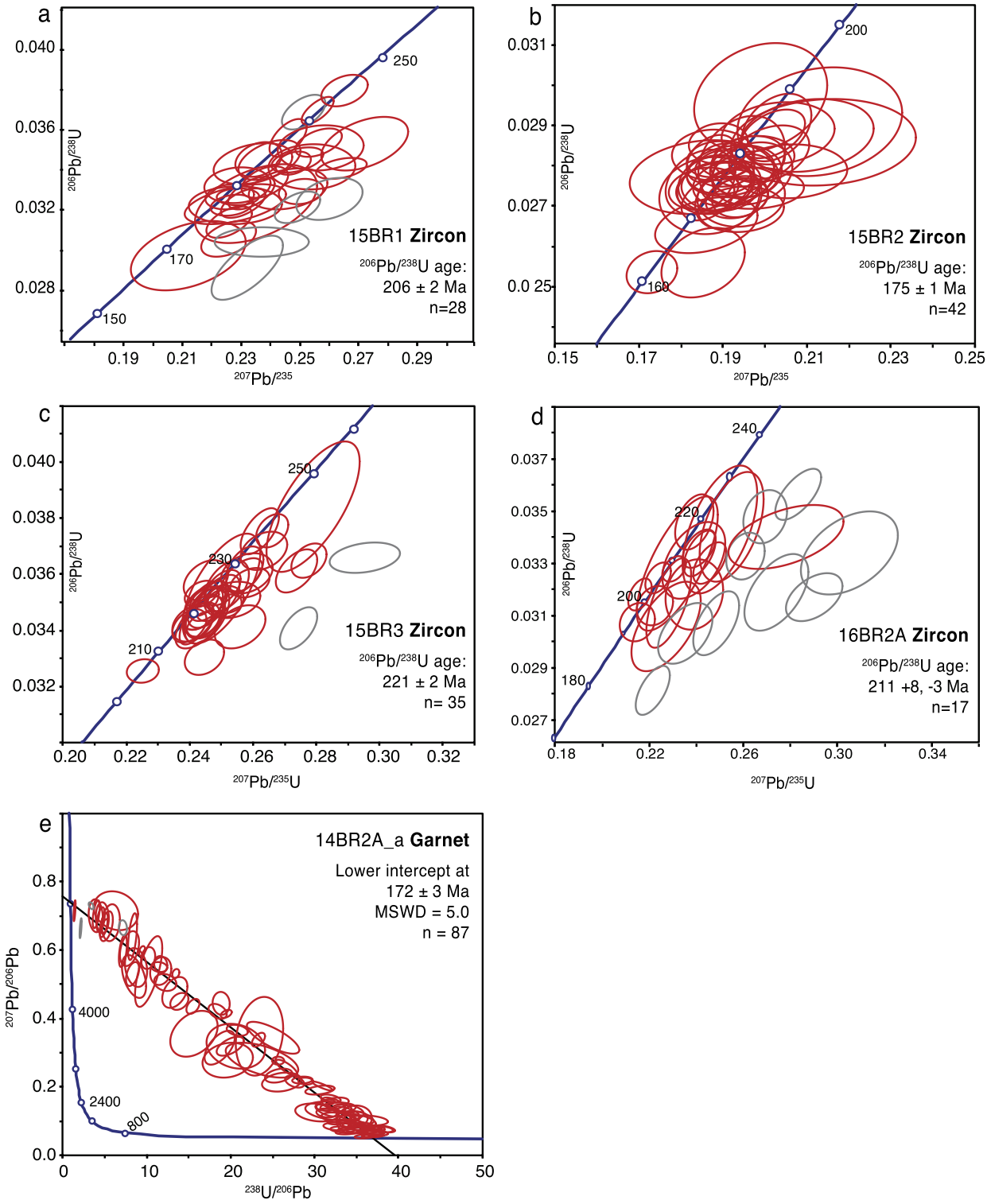

Fig. 6. U–Pb ages associated with the Black Rock Mine skarn. All data-point error analyses are 2σ. (a)–(d) Wetherill Concordia diagrams for zircon separated from plutons in the region of the Black Rock Mine skarn. Grey error ellipses represent analyses with greater than 10% discordance. "n" values refer to the number of concordant analyses. All reported ages are one sigma coherent age populations as calculated by Isoplot, as shown in respective insets. (e) Tera-Wasserberg Concordia diagram for garnet from the Black Rock Mine skarn, Benton Range, CA. Two gray error ellipses are excluded from calculations due to high ratios of ^{206}Pb/^{238}U.

When considering all collected garnet U–Pb spot analysis data, we calculate a skarn garnet U–Pb age of 172 ± 3 Ma with a high MSWD of 5.6. By restricting data to radiogenic analyses with ^{238}U/^{206}Pb greater than 30 and anchoring the ^{207}Pb/^{206}Pb intercept (defined by Discordia based on all data), we calculate an age of 171 ± 2 Ma with a MSWD of 3.7, indicating this over-dispersion is attributable to scatter in the low-radiogenic data yields. Exclusion of low-radiogenic outliers (depicted in gray in Fig. 6e) and recalculation yields an identical age of 172 ± 3 Ma with a slightly improved MSWD of 5.0. This sensitivity of these analyses demonstrates the robustness of the calculated age and attributes the observed over-dispersion primarily to low radiogenic analyses. In

light of these findings, we prefer and report the skarn garnet U–Pb age of 172 ± 3 Ma and MSWD of 5.0 for the Black Rock skarn (Table 1; Fig. 6e), utilizing the most complete and unbiased data array to define the radiogenic lead mixing line and Pbc composition.

Only the Middle Jurassic pluton (15BR_2; Table 2) produces a zircon age that overlaps with the skarn garnet formation age within reasonable error. The high closure temperature of U–Pb in garnet precludes the possibility of thermal resetting, thus we interpret this age determination to represent the age of formation. These ages suggest the Black Rock Mine skarn is genetically related to the magmatism of the ~175 Ma pluton, a conclusion not readily achievable based on field observations alone. This connection between the Black Rock Mine skarn and the 176 Ma pluton provides rational for future investigation of field, geochemical, isotopic, or petrologic evidence in support of a genetic relationship. Matching ages of the Black Rock Mine skarn and causative pluton with those of the Darwin skarn and stock suggest regional plutonism may have been more geographically wide-spread than the solitary Darwin stock suggests.

5.2.2. Application two: dating hydrothermal fluid sources and paleogeographic changes in the Mojave Desert

The Verde Antique and Whitehorse skarns of the Jurassic Mojave arc lie in a geographically important region for studying fluctuations in the tectono-magmatic regime of the southern Jurassic North American Cordillera (Fig. 2). Changes in subduction obliquity and the opening of the Gulf of Mexico result in a transition from extensional tectonics in the Early Jurassic to transtensional dominance in the Late Jurassic (Busby, 2012). The abundant, shallow Jurassic plutons of the Mojave arc are intruded largely into rifted crystalline basement and volcanic rocks during this transition (Busby-Spera et al., 1990; Solomon and Taylor, 1991; Busby, 2012). The influx of fluids with low $\delta^{18}O$ values, interpreted as meteoric in origin, were responsible for high-temperature hydrothermal overprinting of regional plutons (Solomon and Taylor, 1991). These fluids influenced and generated widespread skarn formation at the intersection of these Jurassic plutons and carbonate-rich country rock.

Bulk garnet oxygen isotope data from the Verde Antique and Whitehorse skarns capture the largest amount of variability in $\delta^{18}O$ values documented within an individual skarn system to date, including a preponderance of strongly negative values (−3.7 to +4.4‰ and −9.8 to +2.3‰, respectively; Gevedon et al., 2014). Such low $\delta^{18}O$ values can only result from participation of meteoric surface waters in the active hydrothermal system at the depths of skarn formation. The presence of these fluids at depth has been interpreted to result from the migration of meteoric surface water along the extensional faults responsible for Mojave regional rifting (Solomon and Taylor, 1991; Busby, 2012).

Two individual garnets from the Verde Antique skarn garnetite yield overlapping U–Pb ages of 161 ± 2 Ma (MSWD = 1.6) and 162 ± 2 Ma (MSWD = 1.3; Figs. 7a and 7b; Table 2). A large exoskarn garnet from the Whitehorse skarn with a well-defined core and rim yields an age of 149 ± 5 (MSWD = 1.5; Fig. 7c), which coincides with the youngest known age for regional plutonism (Stone et al., 2013).

The presence of meteoric fluids active in these skarns requires access to surface precipitation, thereby demonstrating that the skarn was above sea level at the time of formation and precluding skarn formation in crust submerged under ocean water. Paleogeographic reconstructions of the Mojave Desert attempt to track the changing position of the shoreline of the paleo-Pacific ocean, which responded to changes in tectonism and latitude through the Early to Middle Jurassic, and eustatic sea-level rise in the Early Cretaceous (Busby, 2012). As such, these new skarn garnet U–Pb ages require that this portion of the Mojave segment of the Jurassic arc had emerged above sea level by the end of the middle Jurassic, earlier than the late-Jurassic emergence suggested by previous oxygen isotope analyses of undated, hydrothermally altered plutons in the region (Solomon and Taylor, 1991). Likewise, these coupled $\delta^{18}O$ values and U–Pb ages provide further support for the

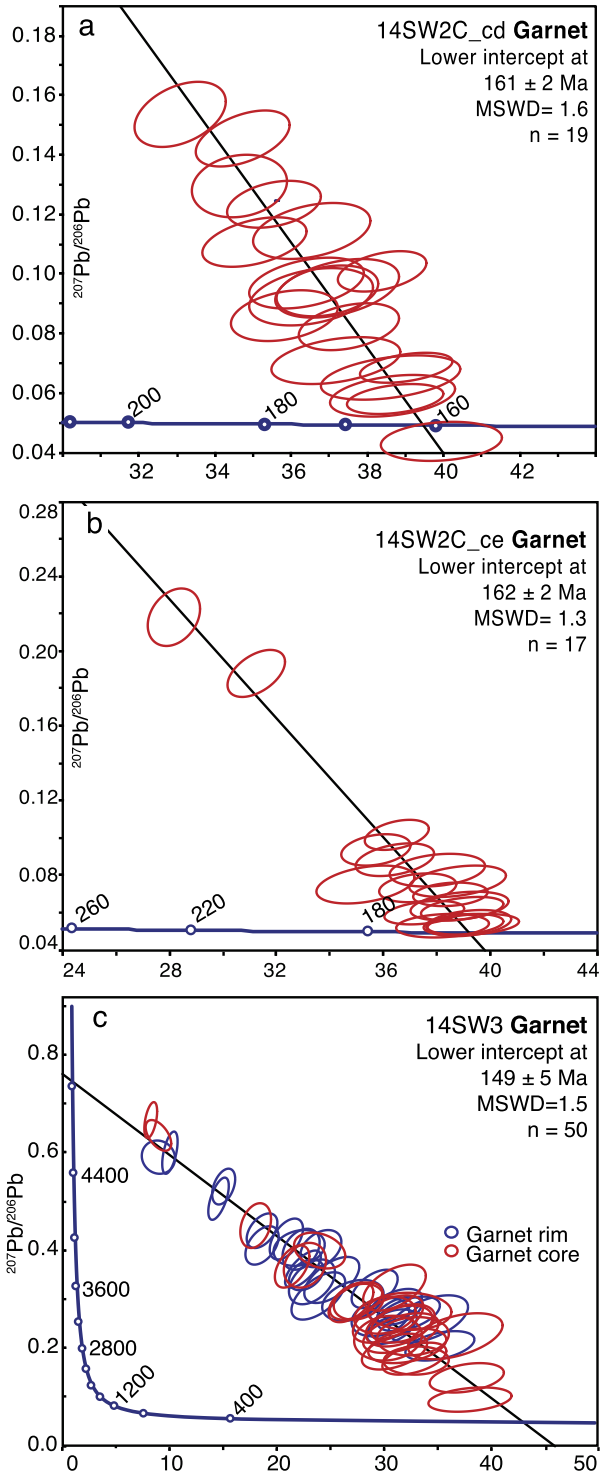

Fig. 7. Select Tera-Wasserberg Concordia (TWC) diagrams depicting individual analytical error ellipses and lower intercept intersection. All data-point error analyses are 2σ. (a) TWC for high-andradite garnet 1 of 2 from the Verde Antique skarn, Mojave Desert, CA. (b) TWC for high-andradite garnet 2 of 2 from the Verde Antique skarn, Mojave Desert, CA. (c) TWC for high-andradite skarn garnet from the Whitehorse skarn, Mojave Desert, CA.

presence of pervasive Jurassic faulting, which provide structural pathways for the delivery of surface waters to skarn formation depths, throughout the north-west Mojave. The Verde Antique and Whitehorse skarn ages indicate that meteoric-based hydrothermal alteration in the Jurassic arc of the Mojave spanned at least 13 Ma (the difference between the oldest and youngest best-fit values of 162 Ma and 149 Ma), suggesting a longer period of hydrothermal activity than previously interpreted (Solomon and Taylor, 1991). In addition, both the Verde Antique and Whitehorse skarns are west of the previously recognized low-δ^{18}O plutons recognized by Solomon and Taylor (1991), thereby expanding the geographic extent of this Mojave low-δ^{18}O zone.

6. Conclusions

Laser-ablation ICP-MS U–Pb dating of andradite-rich skarn garnet can produce geologically robust age constraints for skarn formation independent of the age of associated causative igneous bodies. The ability to U–Pb date andradite-rich garnet provides the future opportunity to determine the temporal relationship between formation of primary skarn minerals and hydrothermal activity relative to emplacement timescales of related magma bodies. Present analytical precision restricts resolution of these timing relationships within the several million year timeframe often indicated for emplacement of plutons of the age range of those chosen in this particular study (i.e., Jurassic and Cretaceous). Analytical precision hinges on the [U] of the analyzed garnet and is demonstrated to correlate with andradite compositions of the analyzed garnet. Laser ablation permits for *in situ* analysis and recovery of spatial age information, such as formation of texturally late garnet rims. As the method continues to improve, it may be possible to date multiple generations of growth within a single skarn. Comparing garnet ages that represent initiation of skarn formation with ages of ore formation (e.g., Re–Os dating of molybdenite) has the potential to reveal whether ore formation directly follows the primary phases of skarn garnet and pyroxene growth, or if ore formation follows a pause in, or reactivation of, hydrothermal activity such as second boiling events (Chesley, 1999; Rasmussen and Mortensen, 2013). Comparison of ore formation ages with skarn garnet formation ages can reveal the duration of active hydrothermal and skarn systems, and if coupled with high-resolution pluton geochronology it may be possible to determine the complex chronologic relationships between hydrothermal activity, ore formation, and the stages of pluton emplacement.

Acknowledgements

We thank E. Kelly, E. Ramos, and M. Odlum for helpful discussions, and L. Stockli and the UTChon Laboratory staff. M. Prior assisted with sample preparation and zircon dating. J. Ryan-Davis assisted with preliminary data collection. M. Cisneros and E. Kelly assisted with EPMA data collection. S. Wafforn assisted with trace element data collection. This work constitutes part of the PhD dissertation of M. Gevedon. We thank anonymous reviewers for their comments, which improved the presentation and focus of previous versions of this paper. This work was funded by NSF-FESD grant 1338842 to J.S.L. and J.D.B.

Appendix A. Supplementary material

Supplementary material related to this article can be found online at https://doi.org/10.1016/j.epsl.2018.06.036.

References

Barth, A.P., Walker, J.D., Wooden, J.L., Riggs, N.R., Schweicker, R.A., 2011. Birth of the Sierra Nevada magmatic arc: Early Mesozoic plutonism and volcanism in the east-central Sierra Nevada of California. Geosphere 7, 877–897.

Bowman, J.R., 1998. Stable-isotope systematics of skarn. In: Lentz, D.R. (Ed.), Mineralized Intrusion-Related Skarn Systems. Mineralogical Association of Canada, pp. 99–145.

Burton, K.W., Kohn, M.J., Cohen, A.S., O'Nions, R.K., 1995. The relative diffusion of Pb, Nd, Sr and O in garnet. Earth Planet. Sci. Lett. 133, 199–211.

Busby, C.J., 2012. Extensional and transtencional continental arc basins: case studies from the southwestern United States. In: Tectonics of Sedimentary Basins: Recent Advances. Blackwell Publishing Ltd., Chichester, UK, pp. 382–404.

Busby-Spera, C.J., 1983. Paleogeographic Reconstruction of a Submarine Volcanic Center: Geochronology, Volcanology and Sedimentology of the Mineral King Roof Pendant, Sierra Nevada, California. Princeton University.

Busby-Spera, C.J., Martinson, J.M., Riggs, N.R., Schermer, E.R., 1990. The Triassic–Jurassic magmatic arc in the Mojave–Sonoran deserts and the Sierran–Klamath region; similarities and differences in paleogeographic evolution. Spec. Pap., Geol. Soc. Am. 255, 325–338.

Cathles, L.M., Erendi, A.H.J., Barrie, T., 1997. How long can a hydrothermal system be sustained by a single intrusive event? Econ. Geol. 92, 766–771.

Chen, J.H., Moore, J.G., 1982. Uranium-lead isotopic ages from the Sierra Nevada Batholith, California. J. Geophys. Res. 87, 4761–4784.

Chesley, J.T., 1999. Integrative geochronology of ore deposits: new insights into the duration and timing of hydrothermal circulation. Rev. Econ. Geol. 12, 115–142.

Coleman, D.S., Gray, W., Glazner, A.F., 2004. Rethinking the emplacement and evolution of zoned plutons: geochronologic evidence for incremental assembly of the Tuolumne Intrusive Suite, California. Geology 32, 433–436.

D'Errico, M.E., Lackey, J.S., Surpless, B.E., Loewy, S.L., Wooden, J.L., Barnes, J.D., Strickland, A., Valley, J.W., 2012. A detailed record of shallow hydrothermal fluid flow in the Sierra Nevada magmatic arc from low-δ^{18}O skarn garnets. Geology 40, 763–766.

Deng, X.D., Li, J.W., Wen, G., 2014. Dating iron skarn mineralization using hydrothermal allanite-(La) U–Th–Pb isotopes by laser ablation ICP-MS. Chem. Geol. 382, 95–110.

Deng, X.D., Li, J.W., Luo, T., Wang, H.Q., 2017. Dating magmatic and hydrothermal processes using andradite-rich garnet U–Pb geochronometry. Contrib. Mineral. Petrol. 172, 1–11.

DeWolf, C.P., Zeissler, C.J., Halliday, A.N., Mezger, K., Essene, E.J., 1996. The role of inclusions in U–Pb and Sm–Nd garnet geochronology: stepwise dissolution experiments and trace uranium mapping by fission track analysis. Geochim. Cosmochim. Acta 60, 121–134.

Elliot, J.E., 1971. The Mineralogy and Chemistry of the Tungsten Deposits of the Black Rock Area, Mono Co., Calif. Stanford Univ., Stanford, CA, p. 90.

Gevedon, M., Ryan-Davis, J., Lackey, J.S., Barnes, J.D., Kitajima, K., Valley, J., 2014. Oxygen isotope zoning in skarn garnets: evidence for spatial and temporal fluid source variability in the Sierra Nevada and Mojave. In: Eos Trans. Am. Geophys. Union. Abstract V33B-4851.

Guo, X., Navrotsky, A., Kukkadapu, R.K., Engelhard, M.H., Lanzirotti, A., Newville, M., Ilton, E.S., Sutton, S.R., Xu, H., 2016. Structure and thermodynamics of uranium-containing iron garnets. Geochim. Cosmochim. Acta 189, 269–281.

Hart, N.R., Stockli, D.F., Hayman, N.W., 2016. Provenance evolution during progressive rifting and hyperextension using bedrock and detrital zircon U–Pb geochronology, Mauléon Basin, western Pyrenees. Geosphere 12, 1166–1186.

Hoskin, P.W., Schaltegger, U., 2003. The composition of zircon and igneous and metamorphic petrogenesis. Rev. Mineral. Geochem. 53, 27–62.

Karish, C.R., Miller, E.L., Sutter, J.F., 1993. Mesozoic tectonic and magmatic history of the central Mojave Desert. Ariz. Geol. Soc. Dig. 18, 15–31.

Levina, M., Horton, B.K., Fuentes, F., Stockli, D.F., 2014. Cenozoic sedimentation and exhumation of the foreland basin system preserved in the Precordillera thrust belt (31–32°S), southern central Andes, Argentina. Tectonics 33, 1659–1680.

Liu, Y., Zhang, R., Zhang, Z., Shi, G., Zhang, Q., Abuduwayiti, M., Liu, J., 2015. Mineral inclusions and SHRIMP U–Pb dating of zircons from the Alamas nephrite and granodiorite: implications for the genesis of a magnesian skarn deposit. Lithos 212, 128–144.

Mathur, R., Marschik, R., Ruiz, J., Munizaga, F., Leveille, R.A., Martin, W., 2002. Age of mineralization of the Candelaria Fe oxide Cu–Au deposit and the origin of the Chilean iron belt, based on Re–Os isotopes. Econ. Geol. 97, 59–71.

McKee, E.H., Conrad, J.E., 1996. A tale of 10 plutons revisited: age of granitic rocks in the White Mountains, California and Nevada. Geol. Soc. Am. Bull. 108, 1515–1527.

Meinert, L.D., 1993. Igneous petrogenesis and skarn deposits. Spec. Pap., Geol. Assoc. Can. 40, 569–583.

Meinert, L.D., Nicolessus, S., Mortenses, J., Cornell, D.H., 2001. U–Pb dating of hydrothermal garnets from skarn deposits: implication for petrogenesis and ore deposits. In: Geological Society of America Annual Meeting. Paper No. 53-50.

Meinert, L.D., Dipple, G.M., Nicolescu, S., 2005. World skarn deposits. Econ. Geol. 100, 299–336.

Mezger, K., Hanson, G.N., Bohlen, S.R., 1989. High-precision U–Pb ages of metamorphic rutile: application to the cooling history of high-grade terranes. Earth Planet. Sci. Lett. 96, 106–118.
Miller, J.S., Matzel, J.E., Miller, C.F., Burgess, S.D., Miller, R.B., 2007. Zircon growth and recycling during the assembly of large, composite arc plutons. J. Volcanol. Geotherm. Res. 167, 282–299.
Nelson, C.A., 1962. Lower Cambrian–Precambrian succession, White-Inyo Mountains, California. Geol. Soc. Am. Bull. 73, 139–144.
Newberry, R.J., 1983. The formation of subcalcic garnet in scheelite-bearing skarns. Can. Mineral. 21, 529–544.
Newberry, R.J., Einaudi, M.T., Eastman, H.S., 1991. Zoning and genesis of the Darwin Pb–Zn–Ag skarn deposit, California: a reinterpretation based on new data. Econ. Geol. 86, 960–982.
Nokleberg, W.J., 1981. Geologic setting, petrology, and geochemistry of zoned tungsten-bearing skarns at the Strawberry Mine, central Sierra Nevada, California. Econ. Geol. 76, 111–133.
Rasmussen, B., Sheppard, S., Fletcher, I.R., 2006. Testing ore deposit models using in situ U–Pb geochronology of hydrothermal monazite: Paleoproterozoic gold mineralization in northern Australia. Geology 34, 77–80.
Rasmussen, K.L., Mortensen, J.K., 2013. Magmatic petrogenesis and the evolution of (F: Cl: OH) fluid composition in barren and tungsten skarn-associated plutons using apatite and biotite compositions: case studies from the northern Canadian Cordillera. Ore Geol. Rev. 50, 118–142.
Romer, R.L., 1992. Vesuvianite-new tool for the U–Pb dating of skarn ore deposits. Mineral. Petrol. 46, 331–341.
Ryan-Davis, J., Lackey, J.S., D'Errico, M., Kitajima, K., Gevedon, M., Barnes, J.D., Lee, C.-T.A., Valley, J.W., 2016. Skarn garnet archives of metasomatic and hydrothermal conditions in the Mineral King roof pendant, South-Central Sierra Nevada. Abstr. Program – Geol. Soc. Am. 48, 4.
Saleeby, J., Dunne, G., 2015. Temporal and tectonic relations of the early Mesozoic arc magmatism, southern Sierra Nevada, California. Spec. Pap., Geol. Soc. Am. 513, 223–268.
Schaltegger, U., Pettke, T., Audétat, A., Reusser, E., Heinrich, C.A., 2005. Magmatic-to-hydrothermal crystallization in the W–Sn mineralized Mole Granite (NSW, Australia): Part I: Crystallization of zircon and REE-phosphates over three million years—a geochemical and U–Pb geochronological study. Chem. Geol. 220, 215–235.
Seman, S., Stockli, D.F., McLean, N.M., 2017. U–Pb geochronology of grossular-andradite garnet. Chem. Geol. 460, 106–116.
Sisson, T.W., Moore, J.G., 2013. Geologic map of southwestern Sequoia National Park, Tulare County, California. US Geological Survey (No. 2013-1096).
Smith, M.P., Henderson, P., Jeffries, T.E.R., Long, J., Williams, C.T., 2004. The rare earth elements and uranium in garnets from the Beinn an Dubhaich Aureole, Skye, Scotland, UK: constraints on processes in a dynamic hydrothermal system. J. Petrol. 45, 457–484.
Solomon, G.C., Taylor, H.P.J., 1991. Oxygen isotope studies of Jurassic fossil hydrothermal systems, Mojave Desert, southeastern California. In: Taylor, H.P.J., O'Neil, J.R., Kaplan, I.R. (Eds.), Stable Isotope Geochemistry: A Tribute to Samuel Epstein. In: Spec. Publ. – Geochem. Soc., pp. 449–462.
Stein, H.J., Markey, R.J., Morgan, J.W., Hannah, J.L., Scherstén, A., 2001. The remarkable Re–Os chronometer in molybdenite: how and why it works. Terra Nova 13, 479–486.
Stein, H., Scherstén, A., Hannah, J., Markey, R., 2003. Subgrain-scale decoupling of Re and 187 Os and assessment of laser ablation ICP-MS spot dating in molybdenite. Geochim. Cosmochim. Acta 67, 3673–3686.
Stone, P., Barth, A.P., Wooden, J.L., Fohey-Breting, N.K., Vazquez, J.A., Priest, S.S., 2013. Geochronologic and Geochemical Data from Mesozoic Rocks in the Black Mounatin Area Northeast of Victorville, San Bernardino County, California. USGS Open-File Report 2013-1146, p. 31.
Tera, F., Wasserburg, G.J., 1972. U–Th–Pb systematics in three Apollo 14 basalts and the problem of initial Pb in lunar rocks. Earth Planet. Sci. Lett. 14, 281–304.
Tornos, F., Delgado, A., Casquet, C., Galindo, C., 2000. 300 million years of episodic hydrothermal activity: stable isotope evidence from hydrothermal rocks of the Eastern Iberian Central system. Miner. Depos. 35, 551–569.
Walker, J.D., Bartley, J.M., Glazner, A.F., 1990. Large-magnitude Miocene extension in the central Mojave Desert: implications for Paleozoic to Tertiary paleogeography and tectonics. J. Geophys. Res. 95, 557–569.
Walker, J.D., Martin, M.W., Glazner, A.F., 2002. Late Paleozoic to Mesozoic development of the Mojave Desert and environs, California. In: Glazner, A.F., Walker, J.D., Bartley, J.M. (Eds.), Geologic Evolution of the Mojave Desert and Southwestern Basin and Range. In: Mem. Geol. Soc. Amer., pp. 1–18. Boulder, Colorado.
Xie, G., Mao, J., Zhao, H., Wei, K., Jin, S., Pan, H., Ke, Y., 2011. Timing of skarn deposit formation of the Tonglushan ore district, southeastern Hubei Province, Middle–Lower Yangtze River Valley metallogenic belt and its implications. Ore Geol. Rev. 43, 62–77.